Taylor & Francis
Taylor & Francis Group

Micro-cracking of brittle polycrystalline materials with initial damage

V. Gulizzi and I. Benedetti 🔟

Dipartimento di Ingegneria Civile, Ambientale, Aerospaziale, dei Materiali (DICAM), Università degli Studi di Palermo, Palermo, Italy

ABSTRACT

In this paper, the effect of pre-existing damage on brittle micro-cracking of polycrystalline materials is explored. The behaviour of single and multiple cracks randomly distributed within a grain scale polycrystalline aggregate is investigated using a recently developed grain boundary 3D computational framework. Each grain is modelled as a single crystal anisotropic domain. Opening, sliding and/or contact at grain boundaries are modelled using nonlinear cohesive-frictional laws. The polycrystalline micro-morphologies are generated using Voronoi tessellation algorithms in combination with a regularisation scheme to avoid the presence of unnecessary small geometrical entities (edges and faces) usually responsible for excessively refined meshes. Additionally, a semi-discontinuous grain boundary mesh within the Boundary Element framework is employed to reduce the computational time and memory storage, while retaining analysis accuracy. To enhance the analysis convergence, a Newton–Raphson scheme is used. The performed numerical tests produce physically sound micro-cracking evolutions, confirming the potential of the technique for multiscale analysis of polycrystalline material damage and failure.

Introduction

Damage nucleation and evolution in brittle polycrystalline materials attract relevant engineering interest, as these materials are used in a wide range of applications, from microelectronics devices to advanced ceramics or armour systems. Understanding their response to applied loads and predicting the crack pattern within their internal microstructure is then crucial in the design of components with specific requirements such as strength, stiffness and toughness.

Polycrystalline materials appear, at the micrometre scale, as an aggregate of crystals with random size and shape, crystallographic orientation and mechanical,

CONTACT I. Benedetti ✉ ivano.benedetti@unipa.it

physical and chemical properties. Thin layers of atoms, the grain boundaries, which have their own properties and act as microstructural discontinuities, separate the crystals. Additionally, flaws such as cracks, voids or precipitates are usually found at the grain boundaries, which then become stress concentration and cracks initiation sites. The ability of including microstructural defect would therefore be desirable to study the behaviour of polycrystalline brittle materials.

At the macroscale, in order to account for a general degradation of the material properties, the usual approach is given by the *continuum damage mechanics*. Such an approach is based on the assumption that cracks, voids and, in general, material flaws, which coalesce and evolve during the loading process, are responsible for the reduction of the elastic moduli of the material. Despite their simplicity, these models are not able to account for the internal microstructure of the considered material, which is in general heterogeneous and has a strong influence on the crack nucleation and evolution.

At the microscale, the failure of brittle polycrystalline materials has been mainly performed using the finite element method (FEM), which remains the most used approach for polycrystalline problems. In a FEM framework, the nucleation, evolution and propagation of cracks within the microstructures are often modelled using a *cohesive zone approach*, based on specific traction-separation laws. In the literature, the most popular cohesive laws are the *intrinsic* laws proposed by Xu and Needleman (1995) and the *extrinsic* laws by Camacho and Ortiz (1996).

Other models for the study of polycrystalline morphologies can be found in the literature. Sukumar, Srolovitz, Baker, and Prévost (2003) employed the extended FEM to study the transition from the intergranular to transgranular crack growth. Raje, Slack and Sadeghi (2009) presented a discrete model in which the crystalline domains are considered as rigid bodies linked with each other through compliant joints. The increasing affordability of high performance computing tools has also paved the way for molecular dynamics simulations of polycrystalline microstructures (Farkas, 2013; Yamakov, Saether, Phillips, & Glaessgen, 2006). However, further developments are needed to bridge the nanoscopic to the macroscopic scale.

As an alternative to the above-mentioned approaches, the Boundary Element Method (BEM) has found application in a wide range of problems (Aliabadi, 2002; Wrobel, 2002). One of the main advantages of the BEM is that it permits to discretise the problem of interest only in terms of boundary variables, thus avoiding the internal volume mesh and therefore reducing the size of the problem itself. In the polycrystalline materials framework, the BEM has been used in combination with the multi-domain technique, in which the primary variables become the intergranular displacements and tractions, facilitating the implementation of the cohesive laws at the grains boundaries. The BEM has been successfully employed for the homogenisation and damage propagation in brittle polycrystalline aggregates for two- (Sfantos & Aliabadi, 2007a) and three-dimensional (Benedetti & Aliabadi, 2013a, 2013b; Gulizzi, Milazzo, & Benedetti, 2015) microstructures. It has been also used to model the degradation of polycrystalline materials in a

two-scale formulation (Benedetti & Aliabadi, 2015; Sfantos & Aliabadi, 2007b). In this work, a boundary element approach (Gulizzi et al., 2015) is used to numerically investigate the effects of initial microstructural imperfections on the aggregate behaviour under progressive quasi-static loading.

The paper is organised as follows. First, the generation of the artificial morphologies in combination with the regularisation scheme proposed by Quey, Dawson, and Barbe (2011) is described. Second, the enhanced grain boundary formulation developed by Gulizzi et al. (2015) is briefly recalled. Third, numerical tests involving polycrystalline microstructures with initial damage are presented to shows the capabilities of the model to include pre-existing damage into the microstructural simulations.

Microstructure generation and grain boundary formulation

In this study, the micro-morphologies are generated using the Hardcore-Laguerre Voronoi tessellation scheme (Fan, Wu, Zhao, & Lu, 2004), which has been widely recognised to reproduce the statistical features of real polycrystalline microstructures in terms of grain size and number of grain's faces. However, typically, the Voronoi scheme tends to produce a large number of small geometrical entities that, although mathematically exact, do not provide any useful information in the simulations of polycrystalline microstructures, thus resulting in a source of unnecessary mesh refinements. To avoid such unwanted issue, the pathological geometrical entities having a length smaller than a predetermined threshold value are removed using the regularisation scheme proposed by Quey et al. (2011). This technique, combined with the enhanced meshing scheme discussed next, ensures a drastic reduction in the number of degrees of freedom for the overall polycrystalline domain, thus leading to a smaller system of equations in terms of memory storage and solution time.

The polycrystalline domain is modelled using the enhanced multi-domain scheme developed by Gulizzi et al. (2015). The grain boundary formulation is briefly recalled here. The generic grain g is considered as a three-dimensional single crystal with general elastic anisotropic behaviour. The displacement and traction fields at the boundaries of the generic grain g are linked through the following boundary integral equations

$$c_{ij}(P)\,u_j(P) + \int_{S_g} T_{ij}(P,Q)\,u_j(Q)\mathrm{d}S(Q) = \int_{S_g} U_{ij}(P,Q)\,t_j(Q)\mathrm{d}S(Q), \quad i,j = 1,2,3 \tag{1}$$

where u_i and t_i are the components of the displacement and traction fields at the grain boundary S_g; P is the generic collocation point where Equation (1) is evaluated; Q is the integration point running over the boundary S_g. $U_{ij}(P,Q)$ and $T_{ij}(P,Q)$ are the fundamental solutions for a generic 3D anisotropic elastic solid

with source point P and field point Q; $c_{ij}(P)$ are the free terms arising from the boundary limiting procedure (Aliabadi, 2002).

In order to discretise the previous integral representation, the grain boundaries are subdivided into a mesh containing triangular and/or quadrangular elements, suitably chosen to minimise the number of degrees of freedom of the grain. Over each mesh element the displacement and the traction fields are approximated using suitable shape functions, which allow to write Equation (1) in the discretised form as follows

$$\mathbf{A}_g \mathbf{X}_g = \mathbf{C}_g \mathbf{Y}_g \qquad (2)$$

where $\mathbf{X}_g$ contains unknown components of displacements and tractions, whereas $\mathbf{Y}_g$ contains the prescribed values (boundary conditions). Accordingly, $\mathbf{A}_g$ and $\mathbf{C}_g$ contain combinations of the columns of the matrices stemming from the integration of Equation (1) (Aliabadi, 2002).

Upon enforcing the intergranular conditions, which will be discussed in detail next, the following system of equations governing the entire polycrystalline aggregate is obtained

$$
\begin{bmatrix}
\mathbf{A}_1 & \mathbf{0} & \cdots & \mathbf{0} \\
\mathbf{0} & \mathbf{A}_2 & \cdots & \mathbf{0} \\
\vdots & \vdots & \ddots & \vdots \\
\mathbf{0} & \mathbf{0} & \cdots & \mathbf{A}_{N_g} \\
\hline
\leftarrow & Interface & Equations & \rightarrow
\end{bmatrix}
\begin{Bmatrix}
\mathbf{X}_1 \\
\mathbf{X}_2 \\
\vdots \\
\mathbf{X}_{N_g}
\end{Bmatrix}
=
\begin{Bmatrix}
\mathbf{C}_1 \mathbf{Y}_1(\lambda) \\
\mathbf{C}_2 \mathbf{Y}_2(\lambda) \\
\vdots \\
\mathbf{C}_{N_g} \mathbf{Y}_{N_g}(\lambda) \\
\mathbf{0}
\end{Bmatrix}
\qquad (3)
$$

where N_g is the number of grains of the aggregate. The interface equations are introduced as additional equations in the system for the overall aggregate. Although they are written as linear relations of the intergranular displacements and tractions, the coefficients of such relations are in general functions of the state and the load history of the grains' interfaces. Finally, on the right-hand side of Equation (3), λ represents the load factor that serves to scale the prescribed boundary conditions.

Boundary conditions

The boundary conditions are applied over the external surfaces of the polycrystalline aggregate and can be given in terms of prescribed displacements, applied stress or in terms of periodic relations between opposite faces of the considered domain (Gulizzi et al., 2015).

Interface conditions

The interface equations relate the displacement and the tractions fields at the interface between two adjacent grains. Calling I_{ab} the interface shared by the grains a and b, the interface equations are written as equilibrium and compatibility equations, which in general are nonlinear expressions of the displacements and tractions at the grain interface. Those equations can be written $\forall x \in I_{ab}$ in the general form

$$
\begin{aligned}
\Psi_i^{ab}\left[\tilde{u}_j^a(x), \ \tilde{u}_j^b(x), \ \tilde{t}_j^a(x), \ \tilde{t}_j^b(x)\right] &= 0 \\
\Phi_i^{ab}\left[\tilde{t}_j^a(x), \ \tilde{t}_j^b(x)\right] &= 0
\end{aligned}
\qquad i, j = 1, 2, 3 \qquad (4)
$$

where Φ_i^{ab} represents the equilibrium condition, whereas, based on the interface state, Ψ_i^{ab} represents either continuity, cohesive or frictional contact laws (Benedetti & Aliabadi, 2013b). In Equation (4) the symbol ˜ denotes quantities calculated with respect to the grain's face local reference system.

It is worth noting that in the present model, it is possible to include general traction-separation laws, which may comprise general anisotropic and nonlinear behaviours. Furthermore, the BEM formulation facilitates the use of the cohesive zone approach, as the primary variables of the model are the intergranular tractions and displacement jumps, which enter directly the intergranular cohesive laws. However, two main challenges remain open: (a) the developed grain boundary model may suffer from numerical instabilities due to the softening behaviour of the traction-separation laws; specific algorithms capable of following the equilibrium path along the softening branch, such as the arc-length procedure (Crisfield, 1981), may be coupled to the model to enhance the numerical solution; (b) there is still the need to suitably identify the parameters entering the cohesive laws, which are usually determined from macroscopic evidences. Grains mis-orientation, inclusions and precipitates, and general non-homogeneities at the grain boundaries are likely to influence the micro-cracking behaviour in terms of crack paths and overall toughness. Methods, such as molecular mechanics and dynamics, able to predict the behaviour of the grain interfaces at the molecular scale, may be used to build more realistic cohesive laws (Zhou, Moody, Jones, Zimmerman, & Reedy, 2009).

Mesh requisite

The mesh size requirements for problems involving cohesive laws have been investigated by Espinosa and Zavattieri (2003b) and Tomar, Zhai, and Zhou (2004) in the FEM framework, and by Sfantos and Aliabadi (2007a) and Benedetti and Aliabadi (2013a) in the BEM framework. They report two factors that must be considered to ensure the mesh independency of the results: (a) the macroscopic

stiffness reduction due to a finite initial stiffness of the cohesive law and (b) the characteristic mesh element length, which must be small enough to capture the stress distribution within the cohesive zone. In this work, using *perfect bonding* equations, i.e. $\delta u = 0$, when the interfacial traction is below a certain threshold value, corresponds to an infinite initial stiffness, which fulfils the requirement (a). With respect to the condition (b), an estimate of the length of the cohesive zone L_{cz} can be given by the following expression (Rice, 1968)

$$L_{cz} \approx \frac{\pi}{2} \left(\frac{K_{IC}}{T_{max}} \right)^2 \tag{5}$$
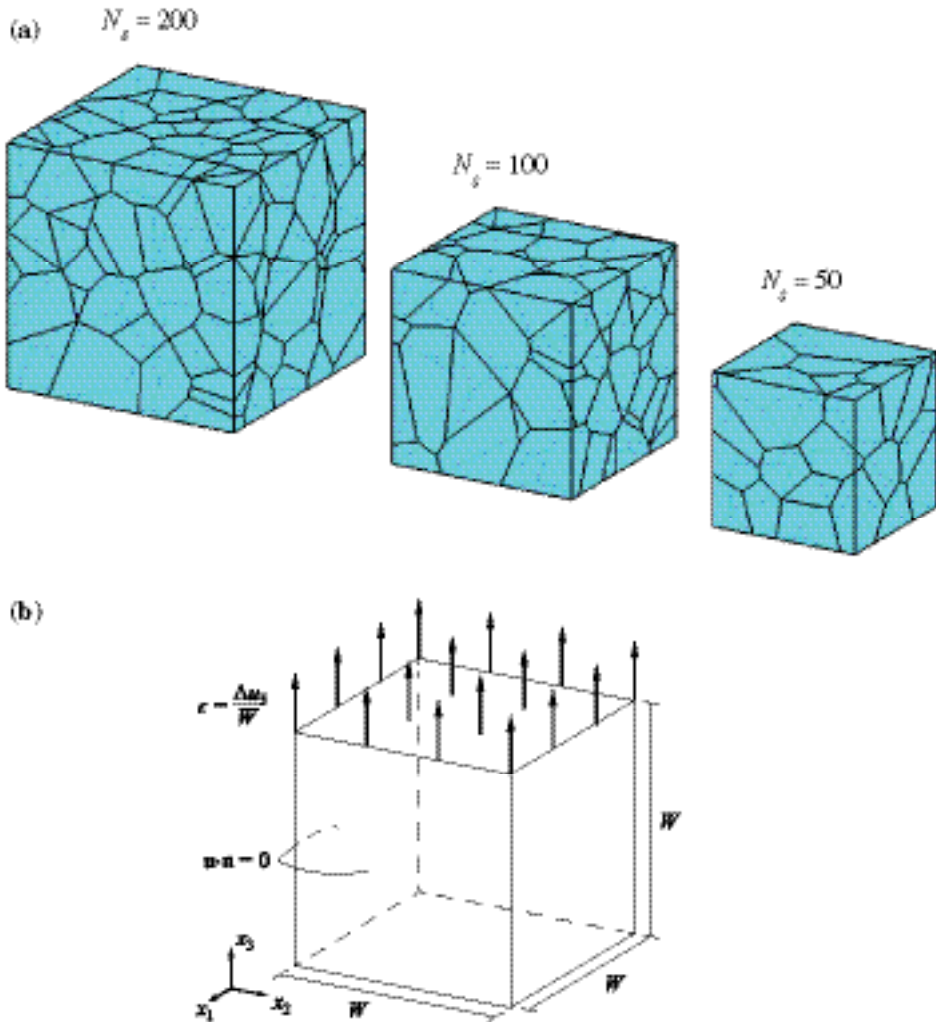
Figure 1. (a) 200-, 100-, and 50-grain morphologies with ASTM grain size $G = 12$ reported to scale. (b) Boundary conditions for the considered morphologies. ϵ is the nominal strain enforced over the top surface as the ratio $\Delta u_3/W$ where W is the side of the cubic aggregates. Over the bottom and the lateral surfaces, the normal displacement is enforced to be zero. n represents the unit normal of the face.

where K_{IC} is the mode I fracture toughness of the material and T_{max} is the threshold stress that triggers the cohesive behaviour of the interface. In this work, to fulfil the requirement (b), the mesh is generated using a uniform mesh size l chosen to ensure the condition $l < L_{cz}$. Using this criterion, Gulizzi et al. (2015) showed that the micro-cracking results obtained using the continuous/semi-discontinuous mesh, combining triangular and quadrangular elements, were in accordance with those obtained by Benedetti and Aliabadi (2013a) using linear discontinuous triangular elements.

System solutions

The system of Equation (3) is solved following the incremental/iterative procedure described by Benedetti and Aliabadi (2013b), where at each load step, the
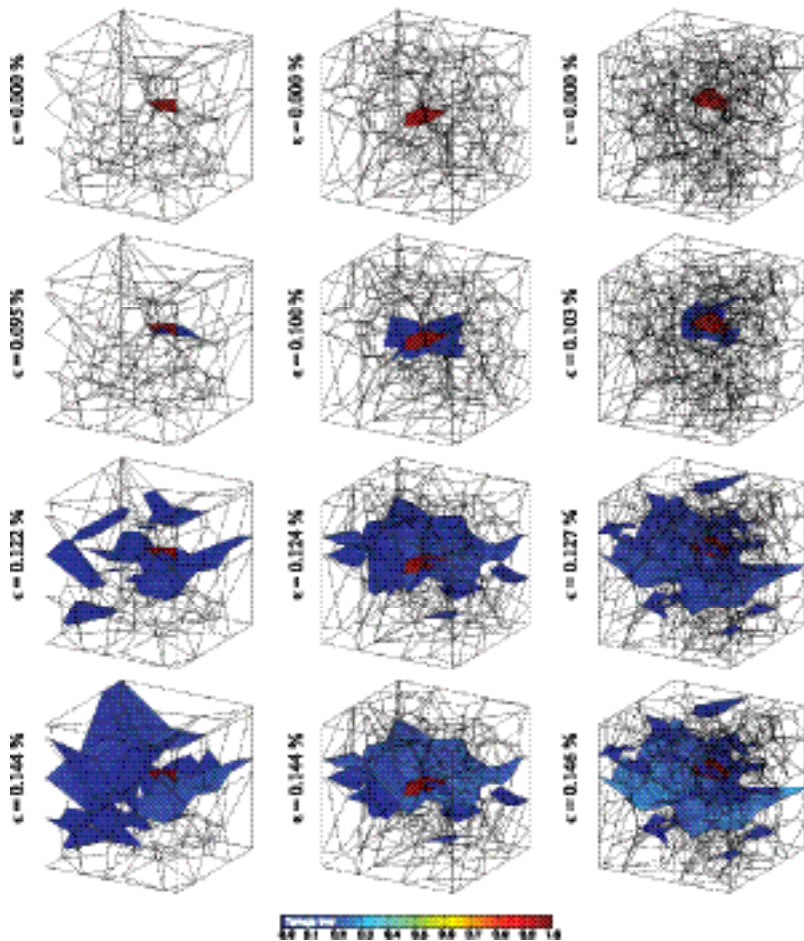
Figure 2. Micro-crack patterns for 50-, 100- and 200-grain morphologies with an embedded crack having a crack area equal to 5% of the base of the polycrystalline domains. (For interpreting the colours, the reader is referred to the web version of the article.)

solution is sought using a Newton–Raphson algorithm to improve the convergence. The system is by construction, highly sparse and the solver PARDISO (Kuzmin, Luisier, & Schenk, 2013; Schenk, Bollhöfer, & Römer, 2008; Schenk, Wächter, & Hagemann, 2007) is used to find the solution. A desirable acceleration of the solution process could be probably obtained employing specialised solvers, based for example on the use of iterative solvers and hierarchical matrices (Benedetti, Aliabadi, & Davì, 2008; Benedetti, Milazzo, & Aliabadi, 2009; Milazzo, Benedetti, & Aliabadi, 2012).

Results

In this section, some case studies are presented to show the effects of initial damage on the micro-cracking response of polycrystalline aggregates. In particular, the effects of a single crack and randomly distributed cracks within the aggregates are discussed.

Single crack behaviour

The case of a pre-existing single crack embedded within a polycrystalline brittle material is presented first. Three morphologies with 50, 100 and 200 grains with ASTM grain size $G = 12$ have been analysed, and are reported in Figure 1(a). The
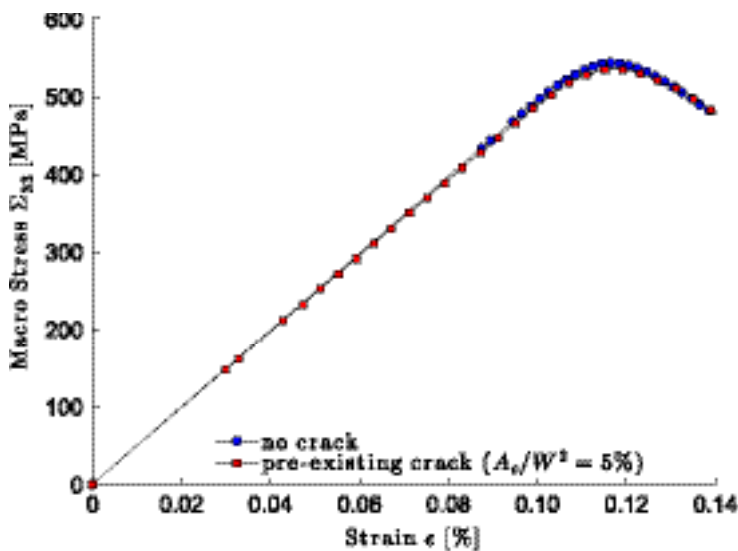

Figure 3. Macroscopic stress–strain curve for the 200-grain morphology subject to tensile load. The figure shows the macroscopic stress vs. the applied nominal strain for a initially intact morphology (blue dots) and a morphology in presence of a pre-existing crack (red squares) with crack area A_c equal to 5% of the base of the aggregate. W indicates the side of the cubic polycrystalline domain. (For interpreting the colours, the reader is referred to the web version of the article.)

morphologies are subjected to a tensile load as shown in Figure 1(b). A nominal strain ϵ is prescribed in terms of the applied displacement u_3 over the top surface. Over the bottom and lateral surfaces the normal displacement is enforced to be zero.

In order to study the behaviour of polycrystalline aggregates in presence of an embedded crack, an interface within the morphologies has been given damage equal to 1, meaning that during tensile loading the interface is not able to carry any load, whereas in compression only sliding governed by
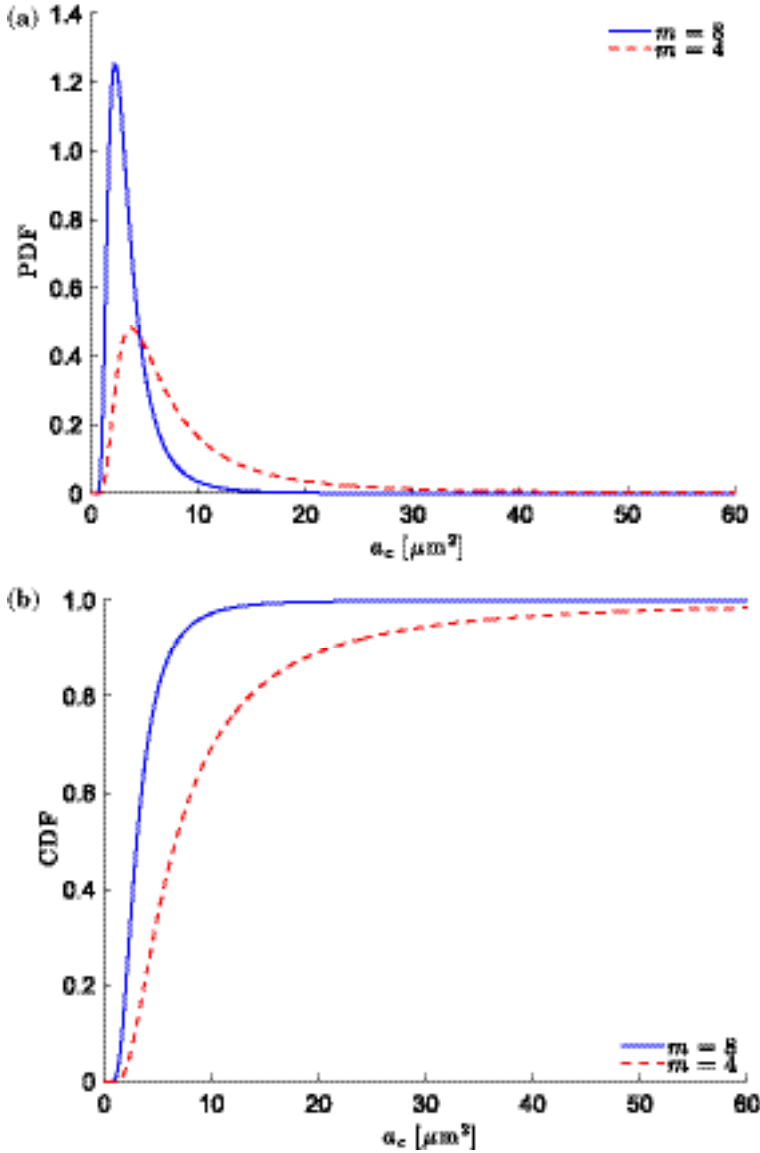

Figure 4. (a) Probability density function (PDF) and (b) cumulative distribution function (CDF) of the crack size distribution for values of the Weibull modulus $m = 4$ and $m = 8$.

the frictional laws (Benedetti & Aliabadi, 2013a) is allowed. The area of the cracked interfaces has been chosen to be 5% of the base of the polycrystalline domains. Figure 2 shows four snapshots of the load history for each of the three morphologies. In the figure, the first, the second and the third column correspond to the 50, 100 and 200-grain morphology, respectively. The first row shows the initial location of the cracks within the aggregates. The damage propagation is then shown per line for different values of the applied nominal strain. It can be noted that, as expected, the presence of the embedded crack drives the initiation of damage, which then propagates towards the boundaries of the polycrystalline domains. However, considering the 50-grain aggregate, it can be seen that the external boundaries have a stronger influence on the final crack pattern with respect to the morphologies with 100 and 200 grains. Finally, Figure 3 reports the macroscopic stress–strain curve for the 200-grain morphology showing that, although driving the crack propagation and final pattern, the presence of such a crack does not heavily influence the macroscopic response.

Randomly distributed cracks

It is experimentally evident that failure of brittle materials is strongly influenced by the presence of randomly distributed defects (cracks, pores, intergranular phases) within their internal microstructure (Espinosa & Zavattieri, 2003a). From a statistical point of view, the strength distribution curves for brittle materials are mathematically well represented by a Weibull distribution. Poloniecki and Wilshaw (1971) showed that the probability density of the crack size distribution in glass could be expressed using the following expression
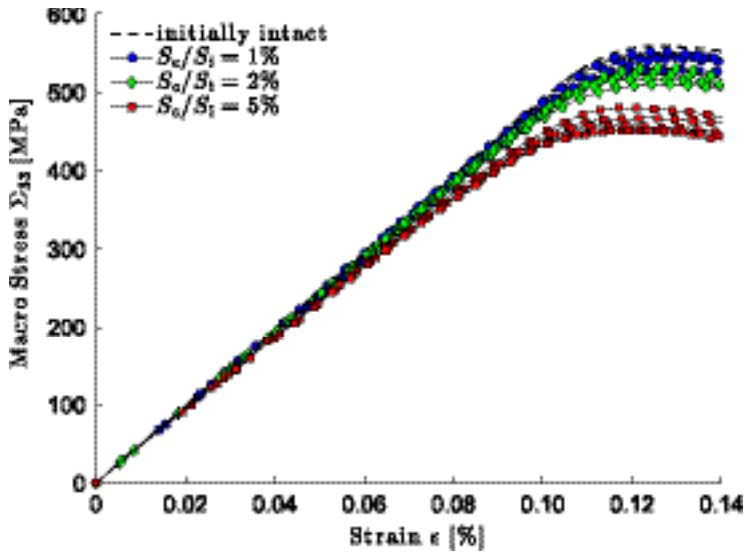
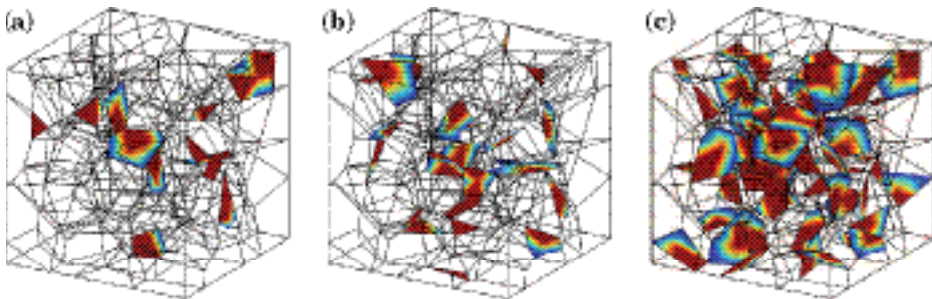$$P(a) = \frac{c^{n-1}}{(n-2)!} a^{-n} \exp\left(-\frac{c}{a}\right) \qquad (6)$$
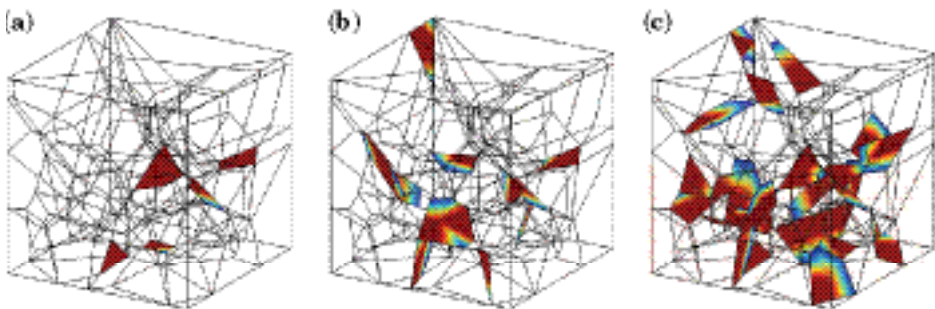
Figure 5. Intergranular crack distribution (Weibull modulus $m = 8$) for a 50-grain morphology (ASTM grain size $G = 12$). Initial cracked grain boundary area equal to (a) 1%, (b) 2% and (c) 5% of the total grain boundary area. The red parts correspond to the cracked interfaces, whereas the blue parts to the intact interfaces. Those interfaces that are not coloured are entirely intact. (For interpreting the colours, the reader is referred to the web version of the article.)

where a is the half-length of the cracks, c is a scaling parameter and n is the rate at which the distribution tends to zero. Such a distribution is related to a Weibull distribution where the Weibull modulus m is obtained as $m = 2n−2$, as shown by Jayatilaka and Trustrum (1977). For brittle ceramics, the Weibull modulus ranges from 3 to 10 (Espinosa & Zavattieri, 2003a).

In this study, pre-existing cracks are inserted within the polycrystalline micro-morphology in terms of the ratio between the cracked grain boundary area, S_c,

Figure 6. Macroscopic stress–strain curve for the 50-grain morphology subject to tensile load. The figure shows the macroscopic stress vs. the applied nominal strain for a initially intact morphology (dotted line) and a morphology in presence of randomly distributed cracks with crack area S_c equal to 1% (blue dots), 2% (green diamonds) and 5% (red squares) of the total grain boundary area S_i. (For interpreting the colours, the reader is referred to the web version of the article.)

Figure 7. Intergranular crack distribution (Weibull modulus $m = 8$) for a 100-grain morphology (ASTM grain size $G = 12$). Initial cracked grain boundary area equal to (a) 1%, (b) 2% and (c) 5% of the total grain boundary area. The red parts correspond to the cracked interfaces, whereas the blue parts to the intact interfaces. Those interfaces that are not coloured are entirely intact. (For interpreting the colours, the reader is referred to the web version of the article.)
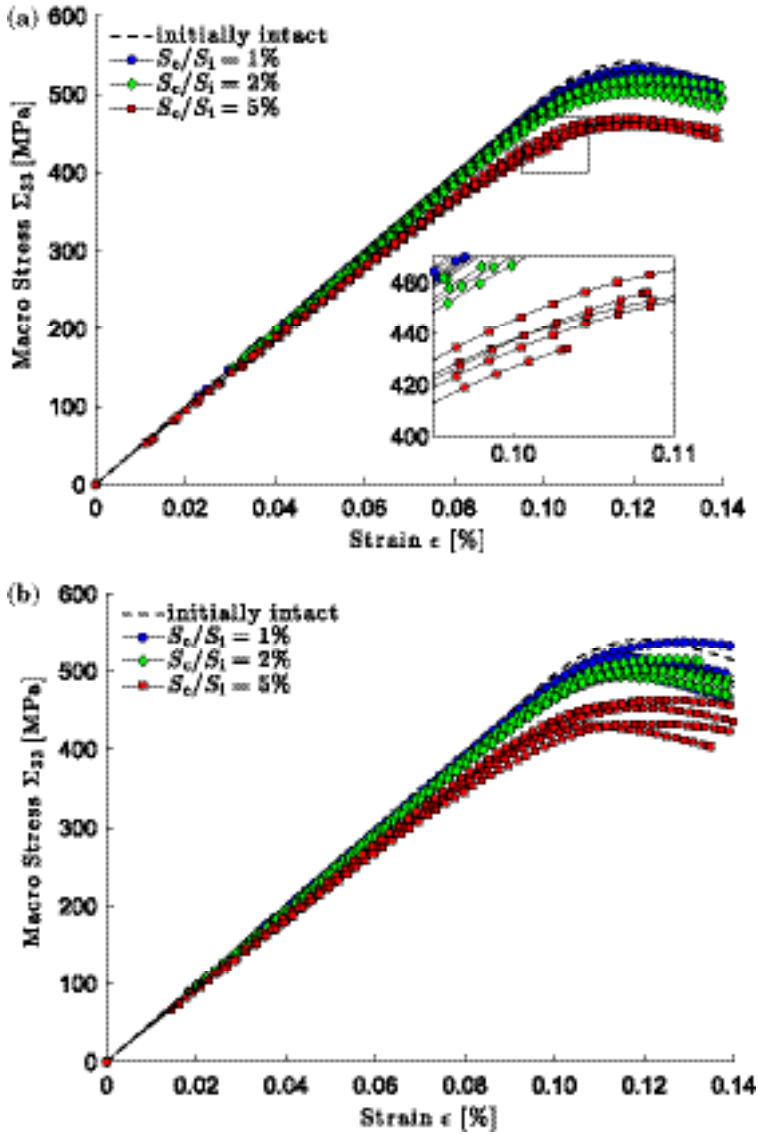
Figure 8. Macroscopic stress–strain curve for the 100-grain morphology subject to tensile load. The figures shows the macroscopic stress vs. the applied nominal strain for a initially intact morphology (dotted line) and a morphology in presence of randomly distributed cracks with (a) Weibull modulus $m = 8$ and (b) Weibull modulus $m = 4$, and crack area S_c equal to 1% (blue dots), 2% (green diamonds) and 5% (red squares) of the total grain boundary area S_i. (For interpreting the colours, the reader is referred to the web version of the article.)

and the total grain boundary area, S_i. The area of the cracked grain boundaries are taken from the distribution described in Equation (6), where a is chosen as the half-side of a square crack, and c as the semi-average grain diameter (Sfantos & Aliabadi, 2007a). Two different values of the Weibull modulus are considered,

Table 1. Average $\bar{\Sigma}_{33}$ and standard deviation $\langle \Sigma_{33} \rangle$ of the tensile strength for the 100-grain morphologies with initial damage distribution.

	Weibull modulus $m = 8$				Weibull modulus $m = 4$			
S_c/S_i	0%	1%	2%	5%	0%	1%	2%	5%
$\bar{\Sigma}_{33}$ [MPa]	541.57	525.41	511.79	455.75	541.57	513.51	501.39	447.21
$\langle \Sigma_{33} \rangle$ [MPa]	–	5.25	8.42	12.97	–	15.15	8.44	16.06

namely $m = 4$ and $m = 8$, whose probability density functions are plotted in Figure 4.

Figure 5 shows the initial distribution with Weibull modulus $m = 8$, of the cracked interfaces within 50-grain polycrystalline aggregates. Figure 5(a)–(c) shows the initial damage distribution for a cracked grain boundary area equal to 1, 2 and 5%, respectively, of the total grain boundary area. For each value of the cracked area, 5 initial cracks distribution have been generated and analysed. The macroscopic stress–strain response is plotted in Figure 6. It can be seen that the presence of initial damage reduces the strength of the polycrystalline domains as the maximum load carried by the domains reduces with increasing values of the initial damaged area.

Similarly to the 50-grain aggregates, Figure 7 shows the initial distribution with Weibull modulus $m = 8$, of the cracked interfaces within 100-grain polycrystalline aggregates. Figure 7(a)–(c) shows the initial damage distribution for a cracked grain boundary equal to 1, 2 and 5%, respectively, of the total grain boundary area. The macroscopic stress–strain responses for the morphologies are then plotted in Figure 8(a). In accordance with the 50 grains tests, the higher the number of cracked interfaces the lower the strength of the polycrystalline morphologies. As shown in the close-up view of Figure 8(a), some of the tests stop to converge before reaching the final prescribed strain. These aggregates are considered as failed at the last computed values of macro-stress. Figure 8(b) shows the macroscopic stress–strain responses for the 100-grain morphologies whose initial damage distribution has been obtained with a Weibull modulus $m = 4$. Table 1 shows the average tensile strength $\bar{\Sigma}_{33}$ and the standard deviation $\langle \Sigma_{33} \rangle$ of the tensile strength for the 100-grain morphologies. As expected, a lower Weibull modulus is responsible for a lower average tensile strength and a higher scatter for the tensile strength of each aggregate.

Conclusions

In this paper, the behaviour of brittle polycrystalline materials in presence of initial damage has been presented. An enhanced grain boundary formulation has been used to model fully three-dimensional polycrystalline domains, which permits to explicitly account for the statistical variability of the internal structures of polycrystalline materials. The model has the advantages of requiring only the discretisation of the grain boundaries and expressing the polycrystalline problems in

terms only of the displacements and tractions at the grain interfaces. Intergranular fracture is then naturally modelled using a suitably defined cohesive law.

The effect of a pre-existing crack on the damage initiation and evolution within polycrystalline domains has been studied for 50, 100 and 200-grain morphologies. The presence of internal cracks randomly distributed accordingly to the Weibull distribution typical of brittle materials, has been also considered, and the link between the damaged interface area and the tensile strength of the aggregates has been highlighted. The performed tests highlight the potential of the model for multiscale analysis of polycrystalline materials degradation and failure.

Acknowledgements

Disclosure statement

No potential conflict of interest was reported by the authors.

ORCID

I. Benedetti ⓘ http://orcid.org/0000-0003-3755-2768

References

Aliabadi, M. H. (2002). *The boundary element method. Volume 2, Applications in solids and structures*. Chichester, West Sussex, England: Wiley.

Benedetti, I., & Aliabadi, M. H. (2013a). A three-dimensional grain boundary formulation for microstructural modeling of polycrystalline materials. *Computational Materials Science, 67*, 249–260. doi:http://dx.doi.org/10.1016/j.commatsci.2012.08.006

Benedetti, I., & Aliabadi, M. H. (2013b). A three-dimensional cohesive-frictional grain-boundary micromechanical model for intergranular degradation and failure in polycrystalline materials. *Computer Methods in Applied Mechanics and Engineering, 265*, 36–62. doi:http://dx.doi.org/10.1016/j.cma.2013.05.023

Benedetti, I., & Aliabadi, M. H. (2015). Multiscale modeling of polycrystalline materials: A boundary element approach to material degradation and fracture. *Computer Methods in Applied Mechanics and Engineering, 289*, 429–453. doi:http://dx.doi.org/10.1016/j.cma.2015.02.018

Benedetti, I., Aliabadi, M. H., & Davì, G. (2008). A fast 3D dual boundary element method based on hierarchical matrices. *International Journal of Solids and Structures, 45*, 2355–2376. doi:http://dx.doi.org/10.1016/j.ijsolstr.2007.11.018

Benedetti, I., Milazzo, A., & Aliabadi, M. H. (2009). A fast dual boundary element method for 3D anisotropic crack problems. *International Journal for Numerical Methods in Engineering, 80*, 1356–1378. doi:http://dx.doi.org/10.1002/nme.2666

Camacho, G. T., & Ortiz, M. (1996). Computational modelling of impact damage in brittle materials. *International Journal of Solids and Structures, 33*, 2899–2938. doi:http://dx.doi.org/10.1016/0020-7683(95)00255-3

Crisfield, M. A. (1981). A fast incremental/iterative solution procedure that handles 'snap-through'. *Computers & Structures, 13*, 55–62. doi:http://dx.doi.org/10.1016/0045-7949(81)90108-5

Espinosa, H. D., & Zavattieri, P. D. (2003a). A grain level model for the study of failure initiation and evolution in polycrystalline brittle materials. Part I: Theory and numerical implementation. *Mechanics of Materials, 35*, 333–364. doi:http://dx.doi.org/10.1016/S0167-6636(02)00285-5

Espinosa, H. D., & Zavattieri, P. D. (2003b). A grain level model for the study of failure initiation and evolution in polycrystalline brittle materials. Part II: Numerical examples. *Mechanics of Materials, 35*, 365–394. doi:http://dx.doi.org/10.1016/S0167-6636(02)00287-9

Fan, Z., Wu, Y., Zhao, X., & Lu, Y. (2004). Simulation of polycrystalline structure with Voronoi diagram in Laguerre geometry based on random closed packing of spheres. *Computational Materials Science, 29*, 301–308. doi:http://dx.doi.org/10.1016/j.commatsci.2003.10.006

Farkas, D. (2013). Atomistic simulations of metallic microstructures. *Current Opinion in Solid State and Materials Science, 17*, 284–297. doi:http://dx.doi.org/10.1016/j.cossms.2013.11.002

Gulizzi, V., Milazzo, A., & Benedetti, I. (2015). An enhanced grain-boundary framework for computational homogenization and micro-cracking simulations of polycrystalline materials. *Computational Mechanics, 56*, 631–651. doi:http://dx.doi.org/10.1007/s00466-015-1192-8

Jayatilaka, A. D. S., & Trustrum, K. (1977). Statistical approach to brittle fracture. *Journal of Materials Science, 12*, 1426–1430. doi:http://dx.doi.org/10.1007/BF00540858

Kuzmin, A., Luisier, M., & Schenk, O. (2013). Fast methods for computing selected elements of the green's function in massively parallel nanoelectronic device simulations. In F. Wolf, B. Mohr, & D. an Mey (Eds.), *Euro-Par 2013 Parallel Processing* (pp. 533–544). Berlin Heidelberg: Springer.

Milazzo, A., Benedetti, I., & Aliabadi, M. H. (2012). Hierarchical fast BEM for anisotropic time-harmonic 3-D elastodynamics. *Computers & Structures, 96*, 9–24. doi:http://dx.doi.org/10.1016/j.compstruc.2012.01.010

Poloniecki, J. D., & Wilshaw, T. R. (1971). Determination of surface crack size densities in glass. *Nature, 229*, 226–227. doi:http://dx.doi.org/10.1038/physci229226a0

Quey, R., Dawson, P. R., & Barbe, F. (2011). Large-scale 3D random polycrystals for the finite element method: Generation, meshing and remeshing. *Computer Methods in Applied Mechanics and Engineering, 200*, 1729–1745. doi:http://dx.doi.org/10.1016/j.cma.2011.01.002

Raje, N., Slack, T., & Sadeghi, F. (2009). A discrete damage mechanics model for high cycle fatigue in polycrystalline materials subject to rolling contact. *International Journal of Fatigue, 31*, 346–360. doi:http://dx.doi.org/10.1016/j.ijfatigue.2008.08.006

Rice, J. R. (1968). Mathematical analysis in the mechanics of fracture. In H. Liebowitz (Ed.), *Fracture: An advanced treatise, mathematical fundamentals* (Vol. 2, pp. 191–311). New York, NY: Academic Press.

Schenk, O., Bollhöfer, M., & Römer, R. A. (2008). On large-scale diagonalization techniques for the anderson model of localization. *SIAM Review, 50*, 91–112. doi:http://dx.doi.org/10.1137/070707002

Schenk, O., Wächter, A., & Hagemann, M. (2007). Matching-based preprocessing algorithms to the solution of saddle-point problems in large-scale nonconvex interior-point optimization. *Computational Optimization and Applications, 36*, 321–341. doi:http://dx.doi.org/10.1007/s10589-006-9003-y

Sfantos, G. K., & Aliabadi, M. H. (2007a). A boundary cohesive grain element formulation for modelling intergranular microfracture in polycrystalline brittle materials. *International Journal for Numerical Methods in Engineering, 69*, 1590–1626. doi:http://dx.doi.org/10.1002/nme.1831

Sfantos, G. K., & Aliabadi, M. H. (2007b). Multi-scale boundary element modelling of material degradation and fracture. *Computer Methods in Applied Mechanics and Engineering, 196*, 1310–1329. doi:http://dx.doi.org/10.1016/j.cma.2006.09.004

Sukumar, N., Srolovitz, D. J., Baker, T. J., & Prévost, J. H. (2003). Brittle fracture in polycrystalline microstructures with the extended finite element method. *International Journal for Numerical Methods in Engineering, 56*, 2015–2037. doi:http://dx.doi.org/10.1002/nme.653

Tomar, V., Zhai, J., & Zhou, M. (2004). Bounds for element size in a variable stiffness cohesive finite element model. *International Journal for Numerical Methods in Engineering, 61*, 1894–1920. doi:http://dx.doi.org/10.1002/nme.1138

Wrobel, L. C. (2002). *The boundary element method, Volume 1, Applications in thermo-fluids and acoustics* (Vol. 1). Chichester, West Sussex, England: Wiley.

Xu, X. P., & Needleman, A. (1985). Numerical simulations of dynamic interfacial crack growth allowing for crack growth away from the bond line. *International Journal of Fracture, 74*, 253–275. doi:http://dx.doi.org/10.1007/BF00033830

Yamakov, V., Saether, E., Phillips, D. R., & Glaessgen, E. H. (2006). Molecular-dynamics simulation-based cohesive zone representation of intergranular fracture processes in aluminum. *Journal of the Mechanics and Physics of Solids, 54*, 1899–1928. doi:http://dx.doi.org/10.1016/j.jmps.2006.03.004

Zhou, X. W., Moody, N. R., Jones, R. E., Zimmerman, J. A., & Reedy, E. D. (2009). Molecular-dynamics-based cohesive zone law for brittle interfacial fracture under mixed loading conditions: Effects of elastic constant mismatch. *Acta Materialia, 57*, 4671–4686. doi:http://dx.doi.org/10.1016/j.actamat.2009.06.023